Acta Crystallographica Section D
Biological Crystallography
ISSN 0907-4449

Structures of D-glyceraldehyde-3-phosphate dehydrogenase complexed with coenzyme analogues

Yue-quan Shen, Shi-ying Song and Zheng-jiong Lin*

National Laboratory of Biomacromolecules, Institute of Biophysics, Chinese Academy of Sciences, Beijing 100101, People's Republic of China

Correspondence e-mail: lin@sun5.ibp.ac.cn

Received 2 January 2002
Accepted 5 June 2002

PDB References: $SNAD^+$–GAPDH, 1ihx, r1ihxsf; ADPR–GAPDH, 1ihy, r1hysf.

Crystal structures of GAPDH from *Palinurus versicolor* complexed with two coenzyme analogues, $SNAD^+$ and ADP-ribose, were determined by molecular replacement and refined at medium resolution to acceptable crystallographic factors and reasonable stereochemistry. ADP-ribose in the ADP-ribose–GAPDH complex adopts a rather extended conformation. The interactions between ADP-ribose and GAPDH are extensive and in a fashion dissimilar to the coenzyme NAD^+. This accounts for the strong inhibiting ability of ADP-ribose. The conformational changes induced by ADP-ribose binding are quite different to those induced by NAD^+ binding. This presumably explains the non-cooperative behaviour of the ADP-ribose binding. Unexpectedly, the $SNAD^+$–GAPDH complex reveals pairwise asymmetry. The asymmetry is significant, including the $SNAD^+$ molecule, active-site structure and domain motion induced by the coenzyme analogue. In the yellow or red subunits [nomenclature of subunits is as in Buehner *et al.* (1974). *J. Mol. Biol.* **90**, 25–49], $SNAD^+$ binds similarly, as does NAD^+ in holo-GAPDH. While, in the green or blue subunit, the $SNAD^+$ binds in a non-productive manner, resulting in a disordered thionicotinamide ring and rearranged active-site residues. The conformation seen in the yellow and red subunits of $SNAD^+$–GAPDH is likely to represent the functional state of the enzyme complex in solution and thus accounts for the substrate activity of $SNAD^+$. A novel type of domain motion is observed for the binding of the coenzyme analogues to GAPDH. The possible conformational transitions involved in the coenzyme binding and the important role of the nicotinamide group are discussed.

1. Introduction

The glycolytic D-glyceraldehyde-3-phosphate dehydrogenase (GAPDH; EC 1.2.1.12) is a tetrameric enzyme that catalyzes the oxidative phosphorylation of D-glyceraldehyde-3-phosphate to form 1,3-diphosphoglycerate in the presence of NAD^+ and inorganic phosphate (Harris & Waters, 1976). The enzyme shows various cooperative properties for binding coenzyme depending on its sources and 'half of the sites' properties, when the SH group of the active-site Cys149 reacts with certain alkylating and acylating reagents (MacQuarrie & Bernhard, 1971; Levitzki, 1974; Ho & Tsou, 1979). Several models have been proposed to explain this cooperative phenomenon (Monod *et al.*, 1965; Bernhard & MacQuarrie, 1973; Koshland *et al.*, 1966).

A number of crystal structures have been solved for GAPDHs. They include those from many mesophilic organisms such as lobsters (Buehner *et al.*, 1974; Moras *et al.*, 1975; Song *et al.*, 1998, 1999; Shen, Li *et al.*, 2000), *Leishmania*

Table 1
Crystal data and structure refinement results.

The crystal of PV holo-GAPDH belongs to same space group as that of ADPR–GAPDH or SNAD$^+$–GAPDH but with different unit-cell parameters: a = 128.40, b = 99.90, c = 80.79 Å, β = 114.48°.

	ADPR–GAPDH	SNAD$^+$–GAPDH
Space group	*C*2	*C*2
Unit-cell parameters (Å, °)	a = 152.81, b = 100.36, c = 128.33, β = 110.27	a = 153.41, b = 100.51, c = 128.44, β = 110.49
Resolution limits (Å)	30.0–3.0	30.0–2.8
No. of subunits per asymmetric unit	4	4
Reflections measured	92755	119278
Unique reflections	35186	44055
$I/\sigma(I)$	7.9 (3.9 for 3.23–3.11 Å, 3.0 for 3.11–3.00 Å)	8.7 (3.5 for 3.02–2.90 Å, 2.4 for 2.90–2.80 Å)
$R_{\rm merge}$ (%)	13.8 (27.0 for 3.23–3.11 Å, 35.0 for 3.11–3.00 Å)	12.6 (30.6 for 3.02–2.90 Å, 37.9 for 2.90–2.80 Å)
Completeness (%)	97 (98.5 for 3.11–3.00 Å)	98 (97.9 for 2.90–2.80 Å)
R factor	0.167	0.169
Free *R* factor (10% of all data)	0.196	0.205
R.m.s. deviations		
Bond lengths (Å)	0.010	0.010
Bond angles (°)	1.40	1.41
Model		
No. of protein atoms	10048	10048
No. of NAD$^+$ analogues	4 ADP-riboses	4 SNAD$^+$
No. of sulfate ions	8	8
No. of water molecules	85	228
Average *B* factors (Å^2)		
Main-chain atoms	25.34	30.71
Side-chain atoms	29.29	33.38
Green subunit	22.84	27.94
Blue subunit	22.05	26.22
Red subunit	31.04	36.14
Yellow subunit	28.95	36.07
NAD$^+$ analogues	82.35	58.60
Solvent	43.78	30.11

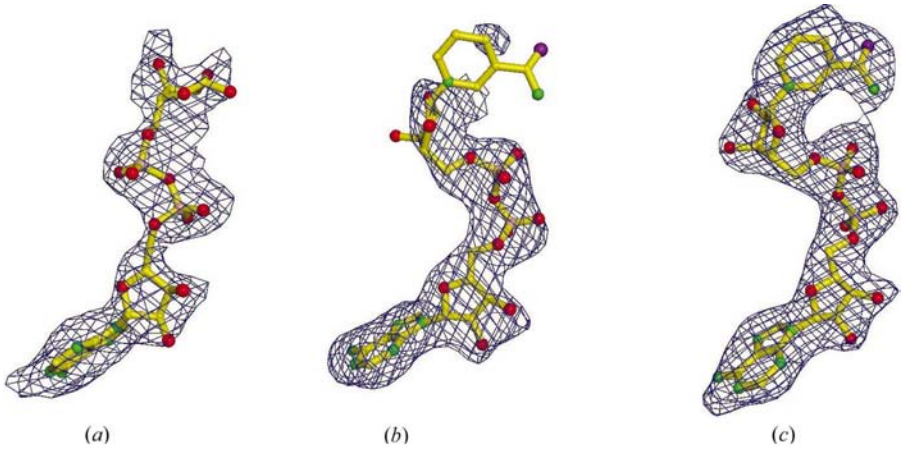

Figure 1
The omit maps of coenzyme analogues: (*a*) ADP-ribose in ADPR–GAPDH; (*b*) SNAD$^+$ in the green or blue subunit of SNAD$^+$–GAPDH; (*c*) SNAD$^+$ in the yellow or red subunit of SNAD$^+$–GAPDH. The contour level is 3σ. The O atoms are shown in red, N atoms in green and S atoms in purple. All figures were prepared using *MOLSCRIPT* (Kraulis, 1991) and *Raster3D* (Merritt & Bacon, 1997).

mexicana (Kim *et al.*, 1995), *Escherichia coli* (Duee *et al.*, 1996), from thermophilic eubacteria such as *Bacillus stearothermophilus* (Skarzynski *et al.*, 1987; Skarzynski & Wonacott, 1988; Didierjean *et al.*, 1997), *Thermotoga maritima* (Korndorfer *et al.*, 1995), *Thermus aquaticus* (Tanner *et al.*, 1996) and from the archaeon *Sulfolobus solfataricus* (Isupov *et al.*, 1999). The active-site structure and the NAD$^+$-induced conformational changes have been observed and the catalytic mechanism of the enzyme has been proposed (Moras *et al.*, 1975; Skarzynski *et al.*, 1987; Song *et al.*, 1999; Duee *et al.*, 1996; Yun *et al.*, 2000). All high-resolution structures of apo- and holo-GAPDH from different sources show good 222 symmetry and tend to support the induced-fit model of the cooperativity.

Several NAD$^+$ analogues have been tested for their enzymatic properties and cooperativity in reactions with rabbit GAPDH (Eby & Kirtley, 1971; Wallen & Branlant, 1983). Two coenzyme analogues, SNAD$^+$ and ADP-ribose, can bind strongly to GAPDH. SNAD$^+$ is effective as a substrate to replace NAD$^+$, and ADP-ribose is a potent competitive inhibitor. They show non-cooperative binding under certain experimental conditions (Eby & Kirtley, 1971; Henis & Levitzki, 1980). In this paper, structures of GAPDH from *Palinurus versicolor* complexed with these two coenzyme analogues (SNAD$^+$–GAPDH and ADPR–GAPDH) are reported and the correlation of these structures with their activity, inhibition and cooperativity are discussed. Unexpectedly, in the SNAD$^+$–GAPDH structure *Q*-axis related subunits remain symmetrical; however, *R*-axis or *P*-axis related subunits reveal significant asymmetry. The possible reasons for the asymmetry are discussed. The enzyme complexes referred to are from the *P. versicolor* enzyme unless otherwise specified. The nomenclature of subunits (green, red, blue, yellow) and the definition of molecular axes (*P*, *Q*, *R*) are the same as those in the *Homarus americanus* GAPDH structure (Buehner *et al.*, 1974). The relationship of the red, green, yellow and blue subunits with the *P*, *Q* and *R* molecular twofold axes is shown in Fig. 6 of this paper. The nomenclature of atoms for NAD$^+$ analogues is same as those for the NAD$^+$ molecule with slight modifications: in SNAD$^+$, NO7→NS7; in ADP-ribose, NN1→NO1* (Skarzynski *et al.*, 1987).

2. Material and methods

2.1. Crystallization, data collection and processing

The holo-GAPDH enzyme was purified from the tail muscle of the South China Sea lobster, *P. versicolor*, according to the method of Allison & Kaplan (1964). The apo-GAPDH enzyme was obtained from the holo-

GAPDH enzyme after the treatment with active charcoal. The crystals of the GAPDH complexes were grown from an equilibrium mixture containing apo-enzyme and the coenzyme analogues as described earlier (Shen, Wang *et al.*, 2000). The crystals of both GAPDH complexes belonged to the same space group *C*2 as holo- or apo-GAPDHs, but with different unit-cell parameters. The asymmetric unit for each of the complex crystals contained one tetramer (four subunits). The data were recorded at 291 K using the MAR Research image plate 345 system to 2.8 Å for SNAD$^+$–GAPDH and to 3.0 Å for ADPR–GAPDH. The data were processed and scaled using *DENZO*/*SCALEPACK* (Otwinowski & Minor, 1997). Crystal and diffraction data statistics are summarized in Table 1.

Table 2
Conformational parameters (°) of NAD$^+$ and NAD$^+$ analogue molecules.

* indicates atoms belonging to ribose rings.

	Angle	NAD$^+$	ADP-ribose	SNAD$^+$ (yellow)	SNAD$^+$ (green)
χ_a	AC4—AN9—AC1*—AO4*	−92.49	−104.37	−107.77	−101.52
γ_a	AC3*—AC4*—AC5*—AO5*	−74.92	−110.75	−61.76	−95.11
β_a	AC4*—AC5*—AO5*—PA	146.63	132.88	151.07	148.89
α_a	AC5*—AO5*—PA—O3	83.52	141.54	7.24	114.54
ζ_a	AO5*—PA—O3—PN	67.30	16.09	104.02	47.07
ζ_n	PA—O3—PN—NO5*	−137.08	154.90	−171.19	−174.70
α_n	O3—PN—NO5*—NC5*	82.42	62.84	47.14	60.49
β_n	PN—NO5*—NC5*—NC4*	157.62	179.94	174.92	175.74
γ_n	NO5*—NC5*—NC4*—NC3*	57.30	179.86	65.97	179.30
χ_n	NO4*—NC1*—NN1—NC2	80.01	—	70.46	—

2.2. Structure determination and refinement

The SNAD$^+$–GAPDH structure was solved by the molecular-replacement method (Rossmann & Blow, 1962) with the program *AMoRe* (Navaza, 1994) using PV holo-GAPDH (PDB code 1szj) as a search model, which is highly homologous to GAPDH from *H. americanus* (sequence identity of 96.4%). The search model consists of the dimer of PV holo-GAPDH made up of the green subunit and its crystallographic twofold-symmetry-related blue subunit (without coenzymes). Two prominent solutions were found for the cross-rotation function with correlation coefficients of 29.5 and 29.4, respectively, for data in the resolution range 8–4 Å (compared with a correlation coefficient of 7.5 for the maximum noise peak). The translation function calculation then yielded two unambiguous solutions with correlation coefficients of 32.5 and 31.3, respectively. The rigid-body fitting resulted in a correlation coefficient of 67.2 and an *R* factor of 0.34. The program *CNS* (Brünger, *et al.*, 1998) was used to refine this model. Firstly, 40 rounds of rigid-body refinements carried out in the data range 30–3.0 Å without non-crystallographic symmetry (NCS) restraints. The $F_o - F_c$ electron-density maps revealed unambiguously the whole SNAD$^+$ molecule in the NAD$^+$-binding site in the yellow and red subunits and only ADP-ribose portion of SNAD$^+$ in the green and blue subunits (Figs. 1*b* and 1*c*). The calculation of SNAD$^+$-induced rotation of NAD$^+$-binding domain relative to the catalytic domain also indicated significant difference between *R*-axis-related subunits or between *P*-axis-related subunits. Obviously, the asymmetry in SNAD$^+$–GAPDH was not induced by the model bias because the initial model (PV holo-GAPDH) used for molecular replacement and the subsequent rigid-body refinement was symmetrical, consisting of four identical subunits. Therefore, *Q*-axis dimer NCS restraints, *i.e.* NCS restraints between the green and blue subunits, and between the yellow and red subunits, were applied [the positional weight constant and σ for the *B* factor are 300 kcal mol^{-1} Å^{-2} and 6.0 Å^2, respectively (1 kcal mol^{-1} Å^{-2} = 4.184 kJ mol^{-1} Å^{-2})] in the following annealing refinement, minimization and individual *B*-factor refinement in order to increase the data-to-parameter ratio.

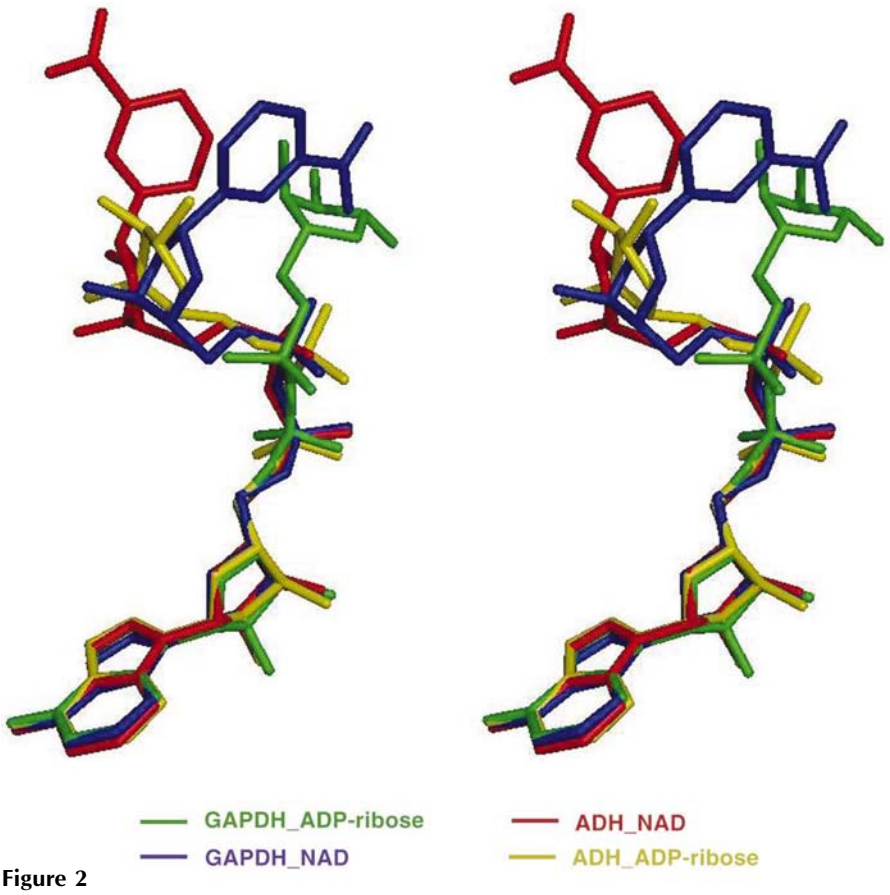

Figure 2
The conformational comparison of ADP-ribose (green) and NAD$^+$ (purple) in GAPDH. The conformations of ADP-ribose (yellow) and NAD$^+$ (red) in ADH are also included.

The data range 30–2.8 Å without cutoff was used in the refinement. In the simulated-annealing procedure, the system was heated to 5000 K and slowly cooled to 300 K in 25 K steps. Based on the $2F_o - F_c$ and $F_o - F_c$ electron-density maps, the SNAD$^+$ molecules, sulfate ions and water molecules were added and the model was further adjusted. 120 rounds of positional refinement and individual *B*-factor refinement were then repeated until the R_{free} factor converged. Manual rebuilding with the graphics program *TURBO-FRODO* (Roussel & Cambillau, 1989) was used when necessary. The final model has an *R* factor of 0.169 and an R_{free} of 0.205. We have also tried other refinement strategies, including those of 222 NCS restraints, *P*-axis dimer NCS restraints, *R*-axis dimer NCS restraints and ignoring NCS; however, all these refinements resulted in models with higher R_{free} factors (above 0.25).

The structural determination and refinement of ADPR–GAPDH were carried out in a similar way to those for SNAD$^+$–GAPDH. After rigid-body refinement without NCS restraints, the tetramer of ADPR–GAPDH still kept good 222 symmetry. The calculated $F_o - F_c$ electron-density map clearly showed the ADP-ribose molecules in the NAD$^+$-binding sites and the similarity of their conformations in all subunits (Fig. 1*a*). On the basis of this, NCS restraints were applied to each subunit (the positional weight constant and σ for the *B* factor are 300 kcal mol^{-1} Å^{-2} and 10 Å^2, respectively). The data range 30–3.0 Å without cutoff was used in the refinement. The final model has an *R* factor of 0.167 and R_{free} factor of 0.196.

The refinement results of both structures are listed in Table 1. The structure determination showed that the SNAD$^+$ and ADP-ribose molecules lying in the NAD$^+$-binding pocket had well defined electron density except the two thionicotinamide groups of SNAD$^+$ in the green and blue subunits, which were not included in the model. The final models of both complexes show good stereochemistry (Table 1). Their Ramachandran plots (Ramachandran *et al.*, 1963) (not shown) are reasonable except for Glu166 and Val237 which are in disallowed regions. The unfavourable geometries of these two residues also existed in many other GAPDH structures. Two sulfate ions per subunit could be found in both structures in positions similar to those in holo-GAPDH.

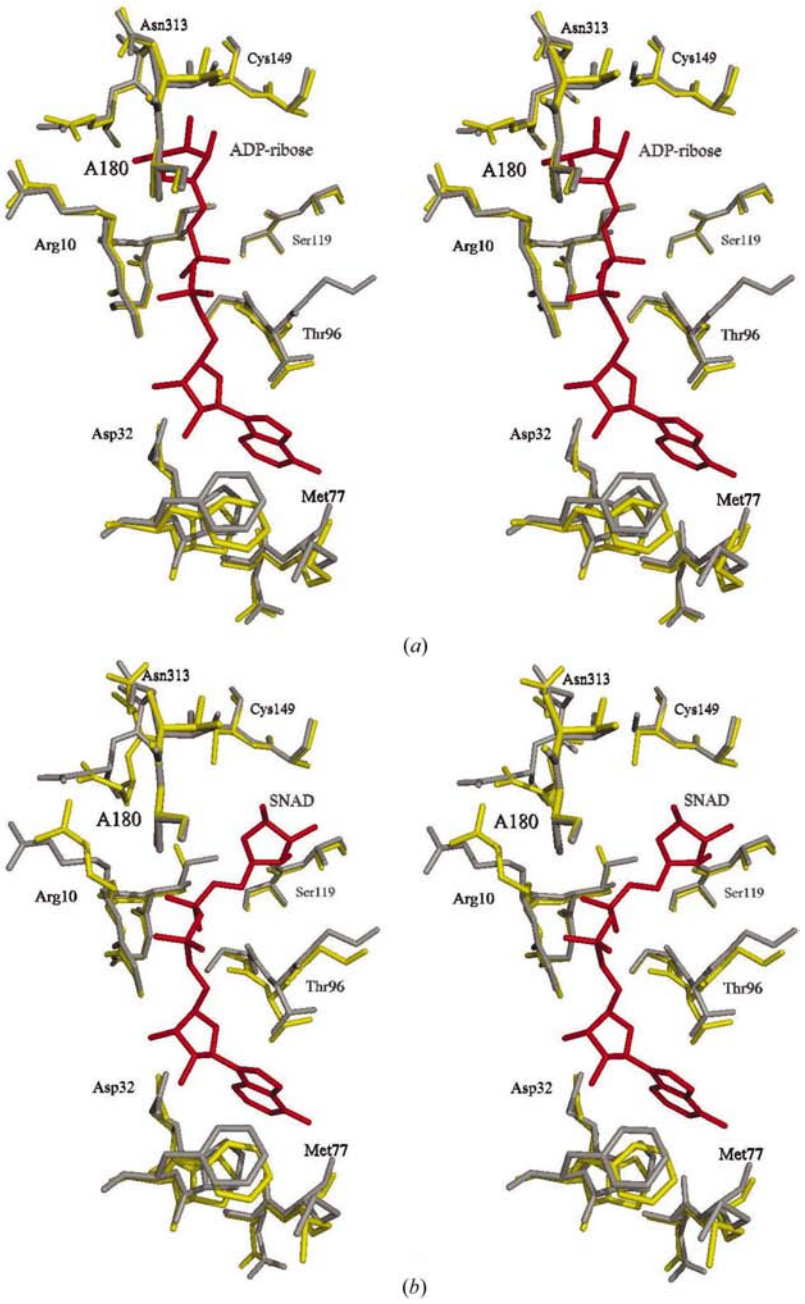

Figure 3
The comparison of NAD$^+$-binding pocket structure of apo-GAPDH (grey) with GAPDH complexes (yellow), showing the conformational changes in the pocket. (*a*) ADPR–GAPDH, (*b*) SNAD$^+$–GAPDH, green or blue subunit, (*c*) SNAD$^+$–GAPDH, yellow or red subunit. The coenzyme analogues are shown in red.

3. Results

As expected, the overall folding and arrangement of subunits in the two GAPDH complexes are essentially similar to those in holo- and apo-GAPDH.

3.1. ADP-ribose binding

The AMP portion of ADP-ribose in ADPR–GAPDH is very similar in overall conformation to the corresponding portion of NAD$^+$ in holo-GAPDH; however, the rest of ADP-ribose differs significantly. The second ribose is not situated on the same side as the adenosine ribose with respect to the diphosphate bridge as observed for NAD$^+$ in holo-GAPDH and in NAD$^+$-ADH and ADP-ribose in ADPR–ADH (Fig. 2). As a consequence, the whole ADP-ribose molecule adopts a rather extended conformation. In the NAD$^+$ of holo-GAPDH,

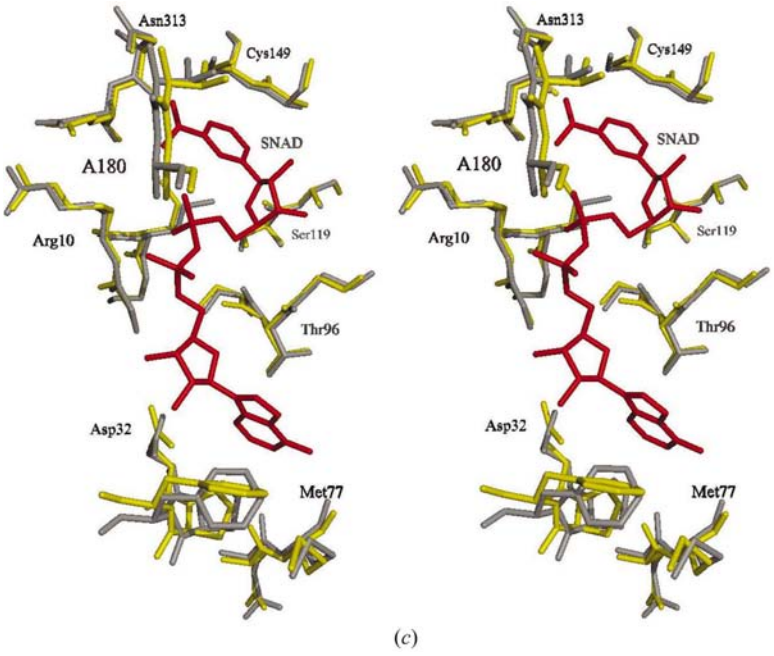

Figure 3 (continued)

the second ribose has to adopt a different conformation so that it is enclosed tightly between the phosphate and the nicotinamide group to avoid the collision between the group and residue Glu314. The distance between the NC2* atom and the AC6 atom in ADP-ribose is 16.15 Å, whereas the corresponding value is 12.85 Å in NAD^+ of holo-GAPDH. The torsion angles for ADP-ribose are listed in Table 2. The substantial difference of second ribose conformation comes from the changes in the torsion angles ξ_n, PA—O3—PN—NO5*, which are −137.08, 154.90 and 102° for holo-GAPDH, ADPR–GAPDH and ADPR–ADH, respectively. This indicates that the pyrophosphate bridge can adopt different geometry depending on the species of the coenzyme analogue and of the enzyme.

ADP-ribose forms a number of polar and hydrophobic interactions with the protein. The hydrogen bonds between the NAD^+ analogue and protein are listed in Table 3. Like the binding mode of the adenosine in holo-GAPDH, the adenine ring forms stable hydrophobic interactions with surrounding residues Pro33, Phe34, Phe99 and Val98, and the adenosine ribose forms hydrophobic interactions with neighbouring residues Phe8, Ile35 and Phe34 and two hydrogen bonds to the side-chain O atoms of Asp32. Significant differences in binding mode occur in the region from the pyrophosphate to the second ribose. This corresponds to the substantial conformational differences between ADP-ribose and NAD^+ there. In ADPR–GAPDH, the NO1* and NO2* atoms of the second ribose form two additional hydrogen bonds with the main-chain N atom of Ala180 in the S-loop from the catalytic domain. In holo-GAPDH, no direct hydrogen bonds are formed between NAD^+ and the catalytic domain.

The structural comparison of ADPR–GAPDH with apo-GAPDH around the coenzyme binding pocket is shown in Fig. 3(*a*) using the superposition based on the NAD^+-binding domain. Residues forming the ADP-ribose binding pocket show different conformational changes from those observed in the comparison of apo- and holo-GAPDH. In the adenosine-binding site, the side chains of Pro33 and Phe34 are shifted outward away from the active site about 1.0 Å and the segment 71–79 is also shifted outward significantly, leading to the increased distance between Met77 O and the ADPR AN6 atom; in the binding site of the second ribose, residue Thr179 moves slightly to avoid close contact with the second ribose. As a result of these movements, ADPR–GAPDH has a slightly more open coenzyme-binding pocket than that in apo-GAPDH.

3.2. $SNAD^+$ binding

In the yellow or red subunit, the overall conformation of $SNAD^+$ in $SNAD^+$–-GAPDH is similar to NAD^+ in holo-GAPDH. The superposition of both the coenzyme and the coenzyme analogue gives an r.m.s.d. value of 0.3 Å only. The substitution of an S atom for an O atom does not have any effect on the general conformation of the nicotinamide group. The planes of the thiocarboxyamide group and the pyridinum ring are inclined at an angle of about 22°, a value close to the corresponding value in the nicotinamide group of holo-GAPDH (Song *et al.*, 1998). The interactions between $SNAD^+$ and the enzyme are also similar to those between NAD^+ and the enzyme (Table 3). In the adenine-binding site, $SNAD^+$ is stabilized by the hydrophobic interactions with the surrounding residues. However, the hydrogen bond, NAD^+ N6A···O Arg77 observed in holo-GAPDH does not exist (3.45 Å), indicating a lesser importance of this hydrogen bond in the binding of $SNAD^+$. Like holo-GAPDH, hydrogen bonds are also found in the Asp32 binding site and the pyrophosphate site. The thionicotinamide-ribose does not make any hydrogen bonds to the protein atoms and only has van der Waals contacts with residues Ile11, Ser95, Gly97, Ser119 and Ala120. The bulky thionicotinamide ring has hydrophobic interactions with Ile11 and Tyr317, forcing a change of the side-chain torsion angles of Ile11. Similar results were also observed in the comparison of apo- and holo-GAPDH from PV and BS (Shen, Li *et al.*, 2000; Skarzynski & Wonacott, 1988). An interesting point is that the carboxamide sulfur NS7 of the thionicotinamide ring can make a weak hydrogen bond with the protein atom Asn313 ND2 (3.24 Å). A similar hydrogen bond, NAD^+ NO7··· ND2 Asn313, in holo-GAPDH has significant importance for productive binding of NAD^+. This interaction was proposed to be an essential structural factor in fixing the nicotinamide ring in the *syn* orientation (Skarzynski *et al.*, 1987; Duee *et al.*, 1996). An NH···S hydrogen bond was reported to exist in thio$NADP^+$–DHFR (McTigue *et al.*, 1993).

In the green and blue subunits, the overall conformation of the ADP-ribose portion of $SNAD^+$ is also similar to the

corresponding portion of NAD^+ in holo-GAPDH but, unexpectedly, the thionicotinamide ring of $SNAD^+$ is disordered and the active-site residues are restructured. Compared with the yellow and red subunits, the side chain of the active-site Cys149 rotates about 90° and residues Glu314 and Arg10 are displaced about 1.5 Å toward Cys149. The movement of these two residues leads to the breakage of the hydrogen bond Arg10 NH1···OD2 Asp47 in the conserved double salt-bridge network, Asp47–Arg10–Glu314 (Fig. 4). The large rotation of Cys149 shows that Cys149 is not activated by His176 and is not correctly located to attack the aldehydic function of the substrate. Therefore, $SNAD^+$ is bound in a non-productive manner on these two subunits.

The structural comparisons of $SNAD^+$–GAPDH with apo-GAPDH around the coenzyme-binding pocket are shown in Fig. 3(*b*) for the green subunit and in Fig. 3(*c*) for the yellow subunit using the same superposition described above. For the yellow or red subunit of $SNAD^+$–GAPDH, most of residues in contact with $SNAD^+$ show conformational changes similar to those found in the comparison of apo- and holo-GAPDH, but to a lesser extent. However, for the green or blue subunit of $SNAD^+$–GAPDH, conformational changes of these residues are similar to those found in the apo-GAPDH and ADPR–GAPDH but to a greater extent. The changes in the latter two subunits involve almost the entire NAD^+-binding domain including the long C-terminal helix. Residues Pro33 and Phe34 have a movement of 1.2 Å toward Cys149 with an accompanying 90° rotation of the Phe34 side chain in the yellow or red subunits, while moving 1.3 Å away from Cys149 in the green or blue subunit. Segment 74–83 has an average 1.0 Å shift toward Cys149 in the yellow or red subunit, while the shift is 1.5 Å away from Cys149 in the green or blue subunit. Thus, the green or blue subunit has an open NAD^+-binding pocket, while the yellow or red subunit is closed.

Table 3
Hydrogen bonds between protein and NAD^+ analogues.

The hydrogen bonds between protein and NAD^+ analogues are similar in all four subunits in ADPR–GAPDH and the values were taken from the green subunit. The corresponding hydrogen bonds are similar in pairs in $SNAD^+$–GAPDH and the values were taken from the yellow and green subunits.

Atom 1	Atom 2	Distance (Å)
ADPR–GAPDH		
ADPR AO3*	Asp32 OD2	3.04
ADPR AO2*	Asp32 OD1	2.73
ADPR AO2*	Asp32 OD2	3.04
ADPR AN6	Met77 O	3.01
ADPR NO1	Ser95 O	3.30
ADPR NO2	Arg10 N	3.14
ADPR NO2	Ile11 N	3.18
ADPR NO2*	Ala180 N	3.37
ADPR NO1*	Ala180 N	3.35
$SNAD^+$–GAPDH (yellow and red)		
$SNAD^+$ AO2	Arg10 N	3.16
$SNAD^+$ AO3*	Asp32 OD2	3.15
$SNAD^+$ AO2*	Asp32 OD1	2.67
$SNAD^+$ AO2*	Asp32 OD2	2.92
$SNAD^+$ NO1	Arg10 N	3.17
$SNAD^+$ NO1	Ile11 N	2.92
$SNAD^+$ NS7	Asn313 ND2	3.24
$SNAD^+$–GAPDH (green and blue)		
$SNAD^+$ AO3*	Asp32 OD2	2.67
$SNAD^+$ AO2*	Asp32 OD1	2.75
$SNAD^+$ AO2*	Asp32 OD2	3.11
$SNAD^+$ NO1	Ser95 O	3.30
$SNAD^+$ NO2	Arg10 N	2.84
$SNAD^+$ NO2	Ile11 N	2.88

3.3. Domain motion

The conformational changes induced by NAD^+ can be described approximately as an overall relative rotation of the two domains accompanying the translation movement of some structural elements. The NAD^+-binding domain rotates about 4° relative to the catalytic domain for BS GAPDH (Skarzynski & Wonacott, 1988) and 3° for PV GAPDH (Shen, Li *et al.*, 2000). In order to study the domain rotation in the two GAPDH complexes, the green subunit was chosen for ADPR–GAPDH and both the green and yellow subunits were chosen for $SNAD^+$–GAPDH (see Fig. 5). The NAD^+-binding domain of ADPR–GAPDH is rotated about 2° relative to the catalytic domain compared with apo-GAPDH. The rotation axis is located at $\varphi = 82$, $\psi = 51$ and $\chi = 358°$, which differ significantly from $\varphi = 130$, $\psi = 140$ and $\chi = 357°$ based on the apo-holo transition. The corresponding rotation for $SNAD^+$–GAPDH can be divided into two classes. For the yellow or red subunit it is about 1.5° with a rotation axis located at $\varphi = 130$, $\psi = 97$ and $\chi = 358.5°$, which is close to that calculated for the apo-holo transition. Unexpectedly, for the green or blue subunit it is about 3° with a rotation axis located at $\varphi = 85$, $\psi = 36$ and $\chi = 357°$, which is close to that calculated for the transition from apo- to ADPR–GAPDH. Therefore, $SNAD^+$–GAPDH shows a 'hybrid'-type domain rotation. This leads to *R* and *P* axis asymmetry in the tetramer of $SNAD^+$–GAPDH as shown in Fig. 6.

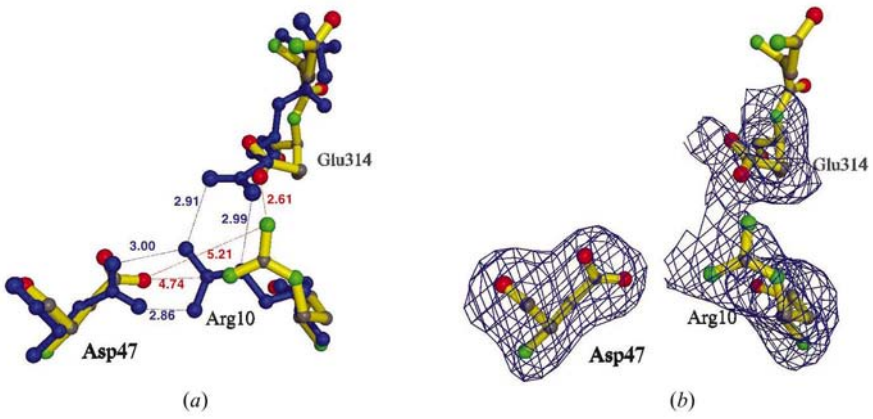

Figure 4
The conformations of ADP-ribose (green) and NAD+ (purple) in GAPDH. As a comparison, the conformations of ADP-ribose (yellow) and NAD^+ (red) in ADH (pdb codes: 5adh and 6adh, Eklund *et al.*, 1984) are also included.

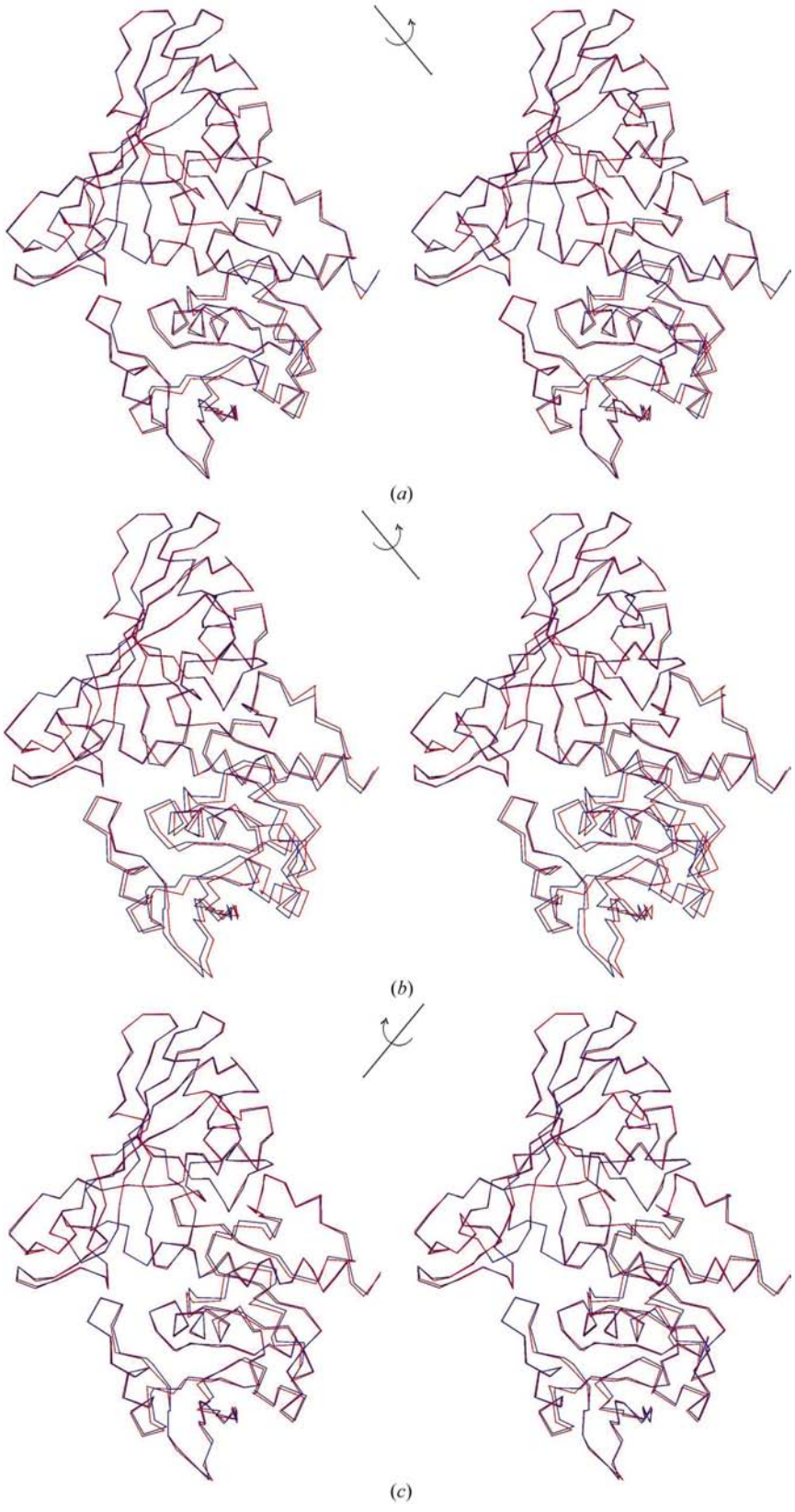

Figure 5
The comparison of subunit structure of apo-GAPDH (blue) with GAPDH complexes (red) using superposition matrix of catalytic domain, indicating the different rotation direction of NAD^+-binding domains. (*a*) ADPR–GAPDH, (*b*) the green or blue subunit of $SNAD^+$–GAPDH, (*c*) the yellow or red subunit of $SNAD^+$-GAPDH. Approximate rotation axis and its rotation direction have been shown in the figures.

3.4. Intersubunit interface

The binding of ADP-ribose and $SNAD^+$ to GAPDH does not significantly affect the subunit interfaces of the tetramer. Hydrogen bonds and ionic bonds within the interfaces for $SNAD^+$–GAPDH are listed in Table 4. As can be seen in the table, the intersubunit interactions at *P* and *R* interfaces are basically the same as those in holo-GAPDH. The hydrogen-bonding interactions (a total of only four) at the *Q* interface are also similar to holo-GAPDH, the only change being the hydrogen bond Asp277 O···OEH Tyr42, which is shortened about 0.3 Å compared with holo-GAPDH owing to the changes in the NAD^+-binding domain. Since the symmetry of the $SNAD^+$–GAPDH tetramer is somewhat distorted, the symmetry at its subunit interfaces is unexpected. The symmetry of intersubunit interactions reflects less the conformational changes induced by the $SNAD^+$ in the β-sheet structure of the catalytic domain and the segment 39–49 of the NAD^+-binding domain, which participate in the intersubunit interactions.

3.5. Crystal packing

The crystal form of the two complexes, *C*2 (II), differs from the crystal form *C*2 (I) reported for holo- and apo-GAPDH from the same source. As shown in Table 1, axes *b* and *c* of *C*2 (II) are approximately equal to the *b* and *a* of *C*2 (I), respectively; however, *a* of *C*2 (II) has twice the length of *c* in *C*2 (I). These results suggest that the molecules in *C*2 (II) may pack with a double-layered *c* face-centred array of *C*2 (I) along *a* of *C*2 (II). The structure analysis confirms this. Fig. 7 illustrates the relationship between the two crystal forms. The unit cell of *C*2 (II) can be simply considered as consisting of two consecutive unit cells of *C*2 (I) along its *c* axis. However, unlike *C*2 (I) where the molecular *Q* axis coincides with crystallographic *b* axis, in *C*2 (II) the molecular *Q* axis is parallel to the plane *ab* and deviates from the crystallographic *b* axis about 4.5°. In *C*2 (II), the *Q* axis is located at $\omega = 90$, $\varphi = -85.5$, $\psi = 180°$; the *P* axis at $\omega = 24$, $\varphi = -175.5$, $\psi = 180°$ and the *R* axis at $\omega = 66$, $\varphi = 5$, $\psi = 180°$ (*LSQAB* from the *CCP*4 program package; Collaborative Computational Project, Number 4, 1994).

From the analysis of the relationship between the two crystal forms, it can be

Table 4
Intersubunit hydrogen bonds and salt bridges in SNAD$^+$-GAPDH.

Atom 1	Atom 2	Distances (Å)
R-axis interface (green–red)		
Tyr39 OH	Ser189 N	2.95
Ser189 N	Tyr39 OH	2.85
Tyr42 OH	Arg197 NH2	3.12
Arg197 NH2	Tyr42 OH	3.30
Ser48 N	Asp186 OD1	2.90
Asp186 OD1	Ser48 N	2.71
Ser48 OG	Asp186 OD1	3.23
Asp186 OD1	Ser48 OG	3.13
Ser48 OG	Asp186 OD2	2.87
Asp186 OD2	Ser48 OG	2.73
Ser48 OG	Arg197 NH1	3.00
Arg197 NH1	Ser48 OG	3.15
Ser48 OG	Asn202 ND2	3.09
Asn202 ND2	Ser48 OG	3.22
Thr49 OG1	Gln201 NE2	3.06
Gln201 NE2	Thr49 OG1	2.92
Thr179 O	Thr184 OG1	2.69
Thr184 OG1	Thr179 O	2.69
P-axis interface (green–yellow)		
Thr173 OG1	Asp241 OD1	2.47
Asp241 OD1	Thr173 OG1	2.38
Thr173 OG1	Lys306 NZ	2.90
Lys306 NZ	Thr173 OG1	2.88
Arg194 NH1	Val278 O	2.85
Val278 O	Arg194 NH1	2.72
Arg194 NH1	Asp293 OD1	2.54
Asp293 OD1	Arg194 NH1	2.80
Arg194 NH2	Asp293 OD2	2.89
Asp293 OD2	Arg194 NH2	2.95
Arg197 NH1	Asp282 OD1	2.66
Asp282 OD1	Arg197 NH1	2.78
Arg197 NH2	Asp282 OD2	2.77
Asp282 OD2	Arg197 NH2	2.81
Asn202 OD1	Cys281 N	2.84
Cys281 N	Asn202 OD1	2.67
Ile203 N	Ser280 OG	2.89
Ser280 OG	Ile203 N	2.92
Q-axis interface (green–blue)		
Tyr42 OH	Asp277 O	2.55
Asp277 O	Tyr42 OH	2.60
Tyr46 OH	Asp276 OD1	2.45
Asp276 OD1	Tyr46 OH	2.48

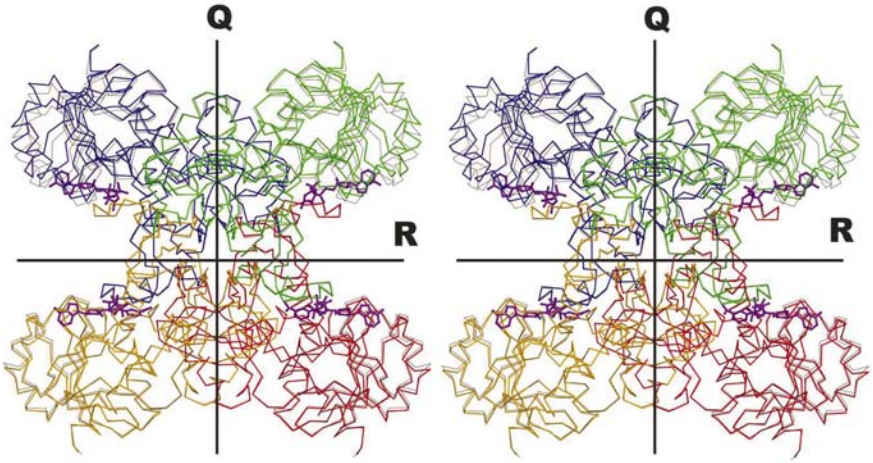

Figure 6
The comparison of subunit structure of holo-GAPDH (black) with SNAD$^+$–GAPDH complexes (green subunit in green, blue subunit in blue, red subunit in red and yellow subunit in yellow) using the superposition matrix of the catalytic domains. The asymmetric structure of SNAD$^+$–GAPDH can be discerned. The *P* axis is vertical to the paper plane.

inferred that the molecular contacts in the crystal form of GAPDH complexed with the coenzyme analogues are basically similar to that of coenzyme free or saturated GAPDH. For the GAPDH tetramer, the NAD$^+$-binding domain usually contributes to the principal tetramer packing as it is located around the periphery of the molecule. In *C*2 (II) crystals, the four NAD$^+$-binding domains have different crystallographic environments. The NAD$^+$-binding domains for the green and blue subunits have multi-point contact regions. The NAD$^+$-binding domain for the red subunit is in contact with only one neighbouring tetramer in one region, involving residue Glu135, which is located at the waist of the subunit. The NAD$^+$-binding domain for the yellow subunit is in contact with two neighbouring tetramers in a similar region around Glu135 and one additional region involving Phe109. Thus, the NAD$^+$-binding domains appear flexible to a certain degree in the yellow and red subunits owing to lesser lattice restriction in comparison with the green and blue subunits, as shown by their higher average *B* factors (see Table 1). This packing feature is similar to that in *C*2 (I) crystals.

4. Discussion

ADP and AMP at high concentration (10^{-3} to 10^{-2} mol l^{-1}) did not break the BS apo-GAPDH crystal but ADP-ribose did even at the lower concentration of 10^{-5} to 10^{-4} *M* (Biesecher *et al.*, 1977). Recently, it was observed, based on the studies of fluorescent changes of Trp84 and Trp310, that significant conformational changes occur in the binding of ADP-ribose to BS apo-GAPDH, while only small conformational changes are generated by AMP or ADP binding (Gabellieri *et al.*, 1996). The crystallographic studies reported here show the details of the interactions between ADP-ribose and apo-GAPDH and the ADP-ribose-induced conformational changes. Such conformational changes, including domain motion, are distinctive and are quite different from those of NAD$^+$-binding. This study indicates that the ADP-ribose moiety alone is insufficient to induce complete NAD$^+$-induced conformational changes and generate the closed state of the subunit because of the lack of a nicotinamide group (in fact, it adopts a slightly more open state than apo-GAPDH). NAD$^+$-induced conformational changes are intimately connected to the cooperativity of GAPDH. The distinctive conformational changes observed in binding of ADP-ribose to GAPDH may be related to its non-cooperative behavior. The ADP-ribose is a potent inhibitor which is competitive with NAD$^+$ for GAPDH. It can be seen from Table 3 that there are nine hydrogen bonds between ADP-ribose and the protein compared with eight hydrogen bonds between NAD$^+$ and the protein. The strong inhibiting ability of

ADP-ribose (K_i = 0.18 mM) can thus be explained by its tight binding to GAPDH.

It is unexpected that SNAD$^+$–GAPDH shows significant structural asymmetry. The thionicotinamide groups of SNAD$^+$ molecules are disordered in half of the subunits (green and blue). The disorder of the thionicotinamide groups observed should not be a consequence of insufficient occupancy of SNAD$^+$ in GAPDH, because of the strong binding ability of SNAD$^+$ to GAPDH (Eby & Kirtley, 1976) and the high concentrations of the analogue in the crystallization solution in comparison with the enzyme (ratio 40:1). The well defined electron density observed for the the ADP-ribose portion reinforces this viewpoint. The flexibility of the nicotinamide ring of NAD$^+$ has been observed in a mutant of GAPDH (Ollivier, 1994). The unique feature found in SNAD$^+$–GAPDH is that the disorder of the thionicotinamide ring only exists in half of the subunits. The structural asymmetry in this complex includes not only the thionicotinamide group but also the active-site-residue arrangement and SNAD$^+$-binding-induced domain motion. Structural asymmetry with respect to the active-site conformation of the GAPDH tetramer has been observed for the structure of the ternary complex trifluoroacetone–NAD$^+$–GAPDH (Garavito *et al.*, 1977). Both of the two structures reveal asymmetry on opposite sides of the *R* molecular axis.

Binding of NAD$^+$ to apo-GAPDH from rabbit or lobster exhibits negative cooperativity. In some cases the binding can be described by assuming two classes of coenzyme binding sites, two tight and two loose sites (Scheek & Slater, 1978; Berni *et al.*, 1979). The appearance of asymmetry in the SNAD$^+$–GAPDH complex seems to support the negative cooperativity of SNAD$^+$ binding or two classes of coenzyme-binding sites. However, it was reported that SNAD$^+$ is non-cooperatively bound on rabbit GAPDH. It is known that the cooperative behaviour of GAPDH varies with enzyme species and experimental pH value (Velick *et al.*, 1971; Niekamp *et al.*, 1977; de Vijlder & Slater, 1968; Reynolds & Dalziel, 1979). The experiments of SNAD$^+$ non-cooperative binding was carried out at a pH of 7.0 for rabbit muscle GAPDH (Eby & Kirtley, 1971), while the crystallization of SNAD$^+$–GAPDH took place at a pH of 6.1 for lobster muscle GAPDH (Shen, Wang *et al.*, 2000). The kinetic experiment of the binding of SNAD$^+$ to PV GAPDH will be helpful in clarifying this issue.

The present SNAD$^+$–GAPDH structure gives unclear indication of structural alterations within the tetramer, which would explain the appearance of asymmetric conformation. It is noted that the four subunits in SNAD$^+$–GAPDH are located in different crystallographic environments; therefore, the differences of subunit conformation in the complex may arise from crystal packing effects. Although the molecular interactions at the crystal contact regions do not directly involve the active site, they may have an effect on the domains orientations and consequently on the conformation of the active site located between the domains. Minor differences in the coenzyme-binding pocket size and domain rotation between the red (or yellow) subunit and the green (or blue) subunit have been observed in the high-resolution structures of apo and holo-GAPDH from the same source and these differences were presumably explained by the crystal packing effect (Shen, Li *et al.*, 2000). The crystal packing of SNAD$^+$–GAPDH is basically similar to those of the apo and holo-GAPDH in spite of differences in crystal form (see §3.5). It is likely that the smaller lattice interactions for the yellow or red subunit in SNAD$^+$–GAPDH allow the coenzyme-binding pockets to accommodate the SNAD$^+$ molecule properly, leading to productive active-site conformation, while the tight lattice interactions for the green or blue subunit fix the domains in a different orientation, thus leading to non-productive active-site conformation. It may be that the green and blue subunits failed to anchor the thioni-

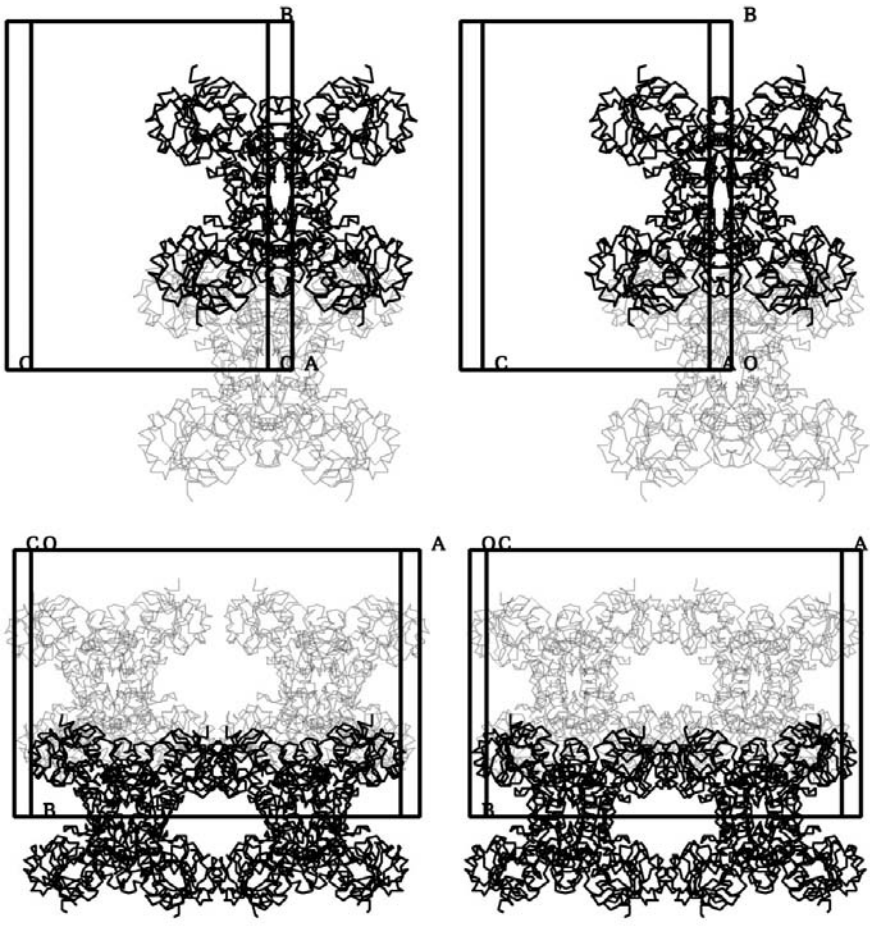

Figure 7
Crystal packing in *C*2 (I) (the crystals of holo-and apo-GAPDH) and *C*2 (II) (the crystals of ADPR–GAPDH and SNAD$^+$–GAPDH).

cotinamide group in its binding site in a precise conformation, resulting in the disorder of the group and this, *vice versa*, forced a rearrangement of surrounding residues in the two subunits. The conformations of SNAD$^+$–GAPDH in the red and yellow subunits may represent those in solution owing to lesser lattice restrictions. On the other hand, the green and blue subunits may adopt conformations not preferred in solution owing to the tight lattice interactions. Similar cases have been reported for other proteins (Gerstein *et al.*, 1994; Rossi, 1992). Releasing the lattice force may induce the formation of a fully productive tetramer GAPDH complex. SNAD$^+$ closely resembles the coenzyme NAD$^+$. The subunit conformational similarity between SNAD$^+$–GAPDH and NAD$^+$–GAPDH and the productive positioning of the pyridinum ring relative to active centre Cys149 as seen in the yellow and red subunits in the crystalline state, explains the substrate activity of the coenzyme analogue.

Structural studies of GAPDH complexed with coenzyme or its analogues so far demonstrate only two distinctive domain motions. One occurs in the apo-holo transition, resulting in a closed state of the NAD$^+$-binding pocket (type II). The other occurs in the transition for ADP-ribose binding, which does not generate the closed state of the NAD$^+$-binding pocket owing to the lack of the nicontinamide ring (type I). The transition for SNAD$^+$ binding has a type II domain motion in the yellow and red subunits, but a type I domain motion in the green and blue subunits owing to the disorder of the thionicontinamide rings in these two subunits. The disorder of the thionicotinamide ring prevents its specific interactions with the protein, including the formation of the important hydrogen bond Asn313 ND2$\cdots$NS7 SNAD$^+$, leading to ADP-ribose-binding-like conformational changes. This underlines the importance of the nicotinamide moiety in completing NAD$^+$-induced conformational transition. In the binding of NAD$^+$ to GAPDH, the ADP portion of NAD$^+$ molecule may firstly bind to a subunit and produce the type I domain motion; the nicotinamide ring of NAD$^+$ then subsequently binds to the subunit and triggers a series of conformational changes (Skarzynski & Wonacott, 1988) and produces a type II domain motion. Therefore, the type I domain motion may represent an intermediate state in the apo-holo transition.

We are grateful for the most valuable suggestions and discussion of Professor Chen-lu Tsou. We would like to thank Dr Li-Chuan Gu for his help in the preparation of this manuscript. This work was supported by China National Natural Science Foundation Grant (No. 39870178).

References

Allison, W. S. & Kaplan, N. O. (1964). *J. Biol. Chem.* **239**, 2140–2152.
Bernhard, S. A. & MacQuarrie, R. A. (1973). *J. Mol. Biol.* **74**, 73–78.
Berni, R., Mozzarelli, A. & Rossi, G. L. (1979). *J. Biol. Chem.* **254**, 8004–8006.
Biesecher, G., Harris, J. I., Thierry, J. C., Walker, J. E. & Wonacott, A. J. (1977). *Nature (London)*, **266**, 328–333.
Brünger, A. T., Adams, P. D., Clore, G. M., Delano, W. L., Gros, P., Grosse-Kunstleve, R. W., Jiang, J. S., Kuszewski, J., Nilges, M., Pannu, N. S. & Read, R. J. (1998). *Acta Cryst.* D**54**, 905–921.
Buehner, M., Ford, G. C., Moras, D., Olsen, K. W. & Rossmann, M. G. (1974). *J. Mol. Biol.* **90**, 25–49.
Collaborative Computional Project, Number 4 (1994). *Acta Cryst.* D**50**, 760–763.
Didierjean, C., Rahuel-Clermont, S., Vitoux, B., Dideberg, O., Branlant, G. & Aubry, A. (1997). *J. Mol. Biol.* **268**, 739–759.
Duee, E., Olivier-Deyris, L., Fanchon, E., Corbier, C., Branlant, G. & Dideberg, O. (1996). *J. Mol. Biol.* **257**, 814–838.
Eby, D. & Kirtley, M. E. (1971). *Biochemistry*, **10**, 2677–2682.
Eby, D. & Kirtley, M. E. (1976). *Biochemistry*, **15**, 2168–2171.
Eklund, H., Samama, J. P. & Jones, T. A. (1984). *Biochemistry*, **23**, 5982–5996.
Gabellieri, E., Rahuel-Clermont, S., Branland, G. & Strambini, G. B. (1996). *Biochemistry*, **35**, 12549–59.
Garavito, R. M., Berger, D. & Rossmann, M. G. (1977). *Biochemistry*, **16**, 4393–4398.
Gerstein, M., Lesk, A. M. & Chothia, C. (1994). *Biochemistry*, **33**, 6739–6749.
Harris, J. I. & Waters, M. (1976). *The Enzymes*, edited by P. D. Boyer, Vol. 13, pp. 1–49. New York: Academic Press.
Henis, I. Y. & Levitzki, A. (1980). *Proc. Natl Acad. Sci. USA*, **77**, 5055–5059.
Ho, Y. -S. & Tsou, C.-L (1979). *Nature (London)*, **277**, 245–246.
Kim, H., Feil, I. K., Verlinde, C. L. M. J., Petra, P. H. & Hol, W. G. J. (1995). *Biochemistry*, **34**, 14975–14986.
Korndorfer, I., Steipe, B., Huber, R., Tomschy, A. & Jaenicke, R. (1995). *J. Mol. Biol.* **246**, 511–521.
Koshland, D. E., Nemethy, G. & Filmer, D. (1966). *Biochemistry*, **5**, 365–385.
Kraulis, P. J. (1991). *J. Appl. Cryst.* **24**, 946–950.
Levitzki, A. (1974). *J. Mol. Biol.* **90**, 451–468.
MacQuarrie, R. A. & Bernhard, S. A. (1971). *J. Mol. Biol.* **55**, 181–192.
McTigue, M. A., Davies, J. F. II, Kaufman, B. T. & Kraut, J. (1993). *Biochemistry*, **32**, 6855–6862.
Merritt, E. A. & Bacon, D. J. (1997). *Method Enzymol.* **277**, 505–524.
Isupov, M. N., Fleming, T. M., Dalby, A. R., Crowhurst, G. S., Bourne, P. C. & Littlechild, J. A. (1999). *J. Mol. Biol.* **291**, 651–660.
Monod, J., Wyman, J. & Changeux, J. P. (1965). *J. Mol. Biol.* **12**, 88–118.
Moras, D., Olsen, K. W., Sabesan, M. N., Buehner, M., Ford, G. C. & Rossmann, M. G. (1975). *J. Biol. Chem.* **250**, 9137–9162.
Navaza, J. (1994). *Acta Cryst.* A**50**, 157–163.
Niekamp, C. W., Sturtevant, J. M. & Velick, S. F. (1977). *Biochemistry*, **16**, 436–445.
Ollivier, R. (1994). PhD thesis, Doctorat de 1'Universite Joseph Fourier Grenoble, France.
Otwinowski, Z. & Minor, W. (1997). *Methods Enzymol.* **276**, 307–326.
Ramachandran, G. N., Ramakrishnan, C. & Sasisekharan, V. (1963). *J. Mol. Biol.* **7**, 95–99.
Reynolds, C. H. & Dalziel, K. (1979). *Biochim. Biophys. Acta*, **567**, 287–94.
Rossi, G. L. (1992). *Curr. Opin. Struct. Biol.* **2**, 816–820.
Rossmann, M. G. & Blow, D. M. (1962). *Acta Cryst.* **15**, 24–31.
Roussel, A. & Cambillau, C. (1989). *TURBO-FRODO. Silicon Graphics Geometry Partner Directory*, edited by Silicon Graphics, pp. 77–78. Mountain View, CA, USA: Silicon Graphics.
Scheek, R. M. & Slater, E. C. (1978). *Biochim. Biophys. Acta*, **526**, 13–24.
Shen, Y.-Q., Li, J., Song, S.-Y. & Lin, Z.-J. (2000). *J. Struct. Biol.* **130**, 1–9.
Shen, Y.-Q., Wang, Z.-J., Song, S.-Y., Zhou, J.-M. & Lin, Z.-J. (2000). *Chin. Sci. Bull.* **45**, 1199–1202.
Skarzynski, T., Moody, P. C. E. & Wonacott, A. J. (1987). *J. Mol. Biol.* **193**, 171–187.

Skarzynski, T. & Wonacott, A. J. (1988). *J. Mol. Biol.* **203**, 1097–1118.
Song, S.-Y., Li, J. & Lin, Z.-J. (1998). *Acta Cryst.* D**54**, 558–569.
Song, S.-Y., Xu, Y.-B. Lin, Z.-J. & Tsou, C.-L. (1999). *J. Mol. Biol.* **287**, 719–725.
Tanner, J. J., Hecht, R. M. & Krause, K. L. (1996). *Biochemistry*, **35**, 2597–2609.
Velick, S. F., Baggott, J. P. & Sturtevant, J. M. (1971). *Biochemistry*, **10**, 779–786.
Vijlder, J. J. de & Slater, E. C. (1968). *Biochim. Biophys. Acta*, **167**, 23–34.
Wallen, L. & Branlant, G. (1983). *Eur. J. Biochem.* **137**, 67–73.
Yun, M., Park, C.-G, Kim, J.-Y. & Park, H.-W (2000). *Biochemistry*, **39**, 10702–10710.